Published in Separation and Purification Technologies 220 (2019) 176-182

Phase stability and oxygen permeability of Fe-based $BaFe_{0.9}Mg_{0.05}X_{0.05}O_3$ (X = Zr, Ce, Ca) membranes for air separation

Guanghu He [a,b], Stefan Baumann [a], Fangyi Liang [b], Heinrich Hartmann [c], Heqing Jiang [b*]
Wilhelm Albert Meulenberg [a*]

[a] Institute of Energy and Climate Research (IEK-1), Forschungszentrum Jülich GmbH, D-52425 Jülich, Germany

[b] Qingdao Key Laboratory of Functional Membrane Material and Membrane Technology, Qingdao Institute of Bioenergy and Bioprocess Technology, Chinese Academy of Sciences, 266101 Qingdao, China

[c] Central Institute for Engineering, Electronics and Analytics (ZEA-3), Forschungszentrum Jülich GmbH, D-52425 Jülich, Germany

* Corresponding authors: jianghq@qibebt.ac.cn, w.a.meulenberg@fz-juelich.de

Published in Separation and Purification Technologies 220 (2019) 176-182

Abstract

The effects of various dopants including Zr^{4+}, Ce^{4+} and Ca^{2+} on the structure and oxygen permeability of B-site doped $BaFe_{0.9}Mg_{0.05}X_{0.05}O_{3-\delta}$ (BFM-X) perovskite-type oxygen transport membranes were studied. Slight X cation doping could stabilize the cubic structure of BFM-X perovskite down to room temperature. XRD, SEM and thermogravimetric results revealed that all the cubic BFM-X oxides exhibited good phase stability under argon atmosphere without any phase changes. The weight loss of BFM-Ce from TG analysis suggests the reduction of cerium ions at high temperatures, which may account for its larger electrical conductivity and higher oxygen permeability comparing to BFM-Zr and BFM-Ca membranes. X-ray photoelectron spectroscopy (XPS) data revealed that Ca dopant with larger size caused the mismatch with Fe ions and led to the substitution of Ca ions at both Fe and Ba site in BFM-Ca oxide, being detrimental to electrical conductivity and oxygen permeation. Among these membranes, BFM-Ce has the highest oxygen permeability and good long term permeation stability under air/argon gradient, thus it was recommended as a potential and promising material for air separation.

Keywords:

Oxygen transport membrane, perovskite, doping, phase stability, oxygen permeability

1. Introduction

Oxygen transport membranes (OTMs), made of mixed ionic-electronic conductors, have attracted considerable attention because of their potential applications in wide areas, such as oxygen separation from air [1, 2], CO_2 capture and utilization [3-5], and chemical reaction coupling with separation process [6, 7]. In the past decades, many OTMs were developed to carry out the above applications. Among them, cobalt-containing perovskite-type (ABO_3) membranes (e.g. $SrCo_{0.8}Fe_{0.2}O_{3-\delta}$) exhibit relatively higher oxygen permeability, since cobalt is beneficial to the activation of oxygen molecules [8, 9]. Even so, only few cobalt-containing membrane materials could be operated steadily either at intermediate temperatures (approximately T = 500 – 800 °C) or under reducing environments (e.g. CH_4, H_2) due to their limited stabilities. Many efforts have been made to develop cobalt-free materials with all desired properties: good oxygen permeability, high thermal and chemical stability, and low cost. For example, Ishihara et al. developed a cobalt-free $LaGaO_3$ based perovskite-type membrane [10]. However, the use of expensive gallium increases the cost significantly and thus limits the large-scale use of this material. Kovalevsky et al. designed another Co-free membrane made of $(Pr_{0.9}La_{0.1})_2(Ni_{0.74}Cu_{0.21}Ga_{0.05})O_{4+\delta}$ with K_2NiF_4-type structure [11], but the oxygen-permeation flux was low (about 0.06 cm^3 min^{-1} cm^{-2} at 800 °C for a membrane thickness of 0.2 μm).

Owing to the better redox stability of iron, Fe-based perovskite-type membranes have been recently approved to be a good alternative to cobalt-containing membranes [12-14]. In particular, we have previously shown that Fe-based $Ba_{0.6}Sr_{0.4}FeO_{3-\delta}$ membranes possessed good oxygen permeability and high phase stability at high temperatures under low oxygen partial pressure atmosphere by Mg-Zr codoping strategy at the B-site of perovskite structure, where the positive aspects of two single-element dopings on oxygen vacancies and tolerance factor of

$Ba_{0.6}Sr_{0.4}FeO_{3-\delta}$ were combined [15]. Generally, partial substitution of B-site cation in perovskite structure with dopant of a large ionic radius can reduce the structural mismatch and stabilize the cubic structure [16-18], on the other hand doping cation with a low valence state can increase the amount of oxygen vacancies in perovskite-type membrane, resulting in a higher oxygen permeability [19, 20]. Therefore, instead of doping Zr^{4+} cation in the previous codoped $Ba_{0.6}Sr_{0.4}FeO_{3-\delta}$ membranes, dopants with larger ionic radii and lower oxidation states than Zr^{4+} should improve the oxygen permeability of the codoped membrane, whilst maintain the phase stability. Among the possible substituents, Ce and Ca have relatively larger size and lower oxidation state than Zr (0.87/1.02 Å/ for Ce^{4+}/Ce^{3+}, 1.0 Å for Ca^{2+}, 0.72 Å for Zr^{4+} in 6-fold coordination) [21] and were able to effectively improve the oxygen permeability of $BaFeO_{3-\delta}$ membranes [18, 22]. Note that the oxidation states of Ce ions in perovskite are variable at high temperature or/and under low oxygen partial pressure atmospheres because of thermal or/and chemical reduction [23, 24].

Following our previous work [15], Ce and Ca were employed as the dopant in the present work to replace Zr in the B-site of codoped perovskite structure for further understanding the codoping effect on the properties of perovskite-type oxygen-transporting membranes. For this purpose, Mg-containing $BaFe_{0.95}Mg_{0.05}O_3$ was taken as the parent perovskite material of which B-site was also doped with Zr, Ce and Ca cations of different oxidation states and ionic radii. The phase stability and oxygen permeability of $BaFe_{0.9}Mg_{0.05}X_{0.05}O_3$ (BFM-X, X= Zr, Ce, Ca) membranes were studied with the emphasis on a possible correlation between dopant property and membrane performance.

2. Experimental

2.1 Powder and membrane preparation

The powders of $BaFe_{0.9}Mg_{0.05}X_{0.05}O_{3-\delta}$ (BFM-X, X=Zr, Ce, Ca) were synthesized by a combined citric acid and ethylene-diamine-tetraacetic acid (EDTA) method. Stoichiometric amounts of nitrates were dissolved in deionized water. Then EDTA and citric acid were added to the nitrate solution at a molar ratio of 1 : 1.5 : 1 to the total of metal cations. The pH value of the solution was adjusted to around 9 using $NH_3 \cdot H_2O$. The solution was subsequently heated with stirring on a heating plate at 120 °C until a dark purple gel formed. After pre-calcination at 600 °C for 5 h, the resultant powder was calcined at 950 °C for 10 h to obtain the powder with the final composition. The calcined powder was uniaxially pressed at 100 MPa into green bodies and sintered in ambient air at 1300 °C for 10 h to form dense membrane disks for oxygen permeation measurements.

2.2 Membrane characterization

The phase composition and crystal structure of BFM-X membranes were analyzed by X-ray diffraction (XRD) using a Bruker D4 ENDEAVOR diffractometer with CuKα in the 20-80° range. In order to evaluate the phase stability of the materials in low oxygen partial pressure atmosphere, the membranes were annealed in a furnace at 900 °C for 24 h in argon. The surface structure and morphology of these membranes before and after annealing were examined using XRD and scanning electron microscopy (SEM, LEO 982), respectively. X-ray photoelectron spectroscopy (XPS) of BFM-Ca membrane fractured in an ultra-high vacuum was also performed on a PHI 5000 Versa Probe II (ULVAC-PHI, Inc) model X-ray photoelectron spectrometer instrument (Al Kα radiation, □ν = 1.486 keV, 50 W). Thermogravimetric analyses

(TGA) of BFM-X oxides were carried out using a NETZSCH STA 449F3 instrument. The powders, loaded in Al_2O_3 crucibles, were heated to 900 °C in dry air atmosphere at a rate of 5 °C min^{-1}. The weight loss behaviors of BFM-X oxides were measured in air and argon atmospheres. The DC four-probe technique was applied to measure the electrical conductivity from 900 to 450 °C in air with a Keithley multimeter (Model 2001). Before measurement, the bar samples (sintered at 1300 °C for 10 h and having a relative density of over 95%) were polished to have a dimension of about 1 × 3 × 16 mm.

2.3 Oxygen permeation measurement

Oxygen permeation studies were carried out using air as feed gas and argon as sweep gas using a lab-scale quartz reactor, which is described in a previous paper [25]. The disc-shape membranes with an open diameter of 13 mm and a thickness of 1 mm were sealed by two gold rings on both sides in the glass tube. All the inlet gas flow rates were controlled by gas mass flow controllers (Bronkhorst, Germany). Air was introduced into the feed side with a flow rate of 250 cm^3 min^{-1} and Ar with a flow rate of 50 cm^3 min^{-1} was swept on the permeate side. The permeated gas was analyzed by a mass spectrometer (Omnistar, Pfeiffer Vacuum). The nitrogen concentration in the permeated gas was also measured to determine the leakage. It is acceptable for permeation measurement when the amount of leakage oxygen is typically less than 1 % of the total amount of the permeated oxygen.

3. Results and discussion

3.1 Crystal structure

The phase composition and crystal structure of the as-prepared BFM-X oxides were characterized by room-temperature XRD as presented in Fig.1. It is well known that perovskite oxides of the composition ABO_3, where A and B denote two different cations, have several lattice symmetries. The ideal structure of perovskite is a cubic lattice, when the ionic size of the A-site cation (12-fold coordination), the B-site cation (6-fold coordination) and the oxygen ion meet the requirement of $r_A + r_O = \sqrt{2}\,(r_B + r_O)$, where r_A, r_B, and r_O are the ionic radii of A site cation, B site cation and oxygen ion, respectively. Although few compounds have this ideal cubic structure, many perovskite oxides have slightly distorted variants with lower symmetry (e.g. hexagonal, orthorhombic, etc.). The deviation from the ideal structure in perovskite oxides is expressed through tolerance factor, *t*:

$$t = \frac{r_A + r_O}{\sqrt{2}(r_B + r_O)} \qquad \text{(eq.1)}$$

When the tolerance factor is greater than 1.0, a hexagonal structure tends to form. As shown in Fig.1, the single Mg element doped $BaFe_{0.95}Mg_{0.05}O_{3-\delta}$ oxide displays a hexagonal perovskite structure of which the tolerance factor is 1.036 or 1.065 estimated assuming Fe in the valence of Fe^{3+} (HS, 0.645 Å) or Fe^{4+} (0.585 Å), respectively. This observation is quite common for perovskite oxides with a large mismatch in the size of A and B site cations [16]. Surprisingly, only 5 mol.% of X ion (i.e., Zr, Ce, Ca) doped at the B-site of $BaFe_{0.95}Mg_{0.05}O_{3-\delta}$ was able to transform the hexagonal structure to cubic perovskite structure without any detectable impurity, suggesting that X dopant is dissolved into the host material BFM. As mentioned before, the radii of Zr^{4+}, Ce^{4+} and Ca^{2+} are all larger than Fe ion [21], indicating that the tolerance factor of

codoped BFM-X perovskite decreases gradually to the unity with increasing the radius of X ion from Zr to Ca. In addition, the doping of these ions would result in an expansion of the BFM unit cell, and this expansion is reflected by the XRD peak shift to the small angle regions gradually (Fig.1). It should be noted here that XRD peaks of BFM-Ca membrane further shift toward the small angle regions compared to that of Zr-doped and Ce-doped membranes, indicating that the lattice parameter of Ca-doped BFM is the largest among the BFM-X oxides. Consequently, the Ca^{2+} dopants are mainly occupying the B-site of BFM-Ca structure because A-site doping on the larger Ba^{2+}-sites would presumably lead to smaller lattice parameters. It is also noted that $BaFe_{0.9}Mg_{0.05}Zr_{0.05}O_{3-\delta}$ (BFM-Zr) is a cubic perovskite while $BaFe_{0.9}Mg_{0.1}O_{3-\delta}$ (BFM) has a hexagonal phase although the radius of Mg^{2+} (0.72 Å) is the same as that of Zr^{4+} (0.72 Å), which is similar to the observation of Zn^{2+} doped $SrCo_{0.95}Zn_{0.05}O_{3-\delta}$ and Sc^{3+} doped $SrCo_{0.95}Sc_{0.05}O_{3-\delta}$ [26]. These observations suggest that the valence state of dopant has an influence on the crystal structure of perovskite. In summary, the XRD studies indicate that all dopants including Zr, Ce and Ca ions were incorporated at the B-site of BFM with reducing the mismatch between Ba and Fe cations. As a result, the phase transition to a cubic perovskite structure occurs.

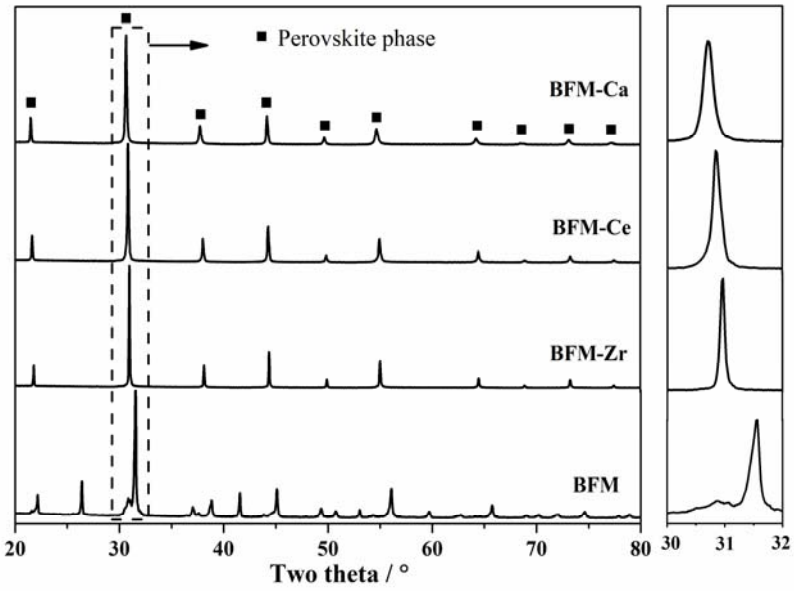

Fig. 1. XRD patterns of as-prepared BFM-X membrane sintered at 1300 °C for 10 h

It is well known that the ionic radii of dopants have significantly affected on their site occupancy in perovskite structure [27-29]. Taking $BaZr_{0.8}M_{0.2}O_{3-\delta}$ (M = Sc, Eu, Sm, Dy) as examples, Sc cation having a radius comparable with that of Zr cation only occupied the B-site of $BaZrO_3$. However, relatively larger Eu, Sm and Dy cations occupied both the A- and B-site of $BaZrO_3$ [27]. The radius of 6-fold coordinated Ca^{2+} is 1.0 Å, which is much larger than that of Fe ion. So, the site occupancy of Ca cation in BFM was evaluated using XPS measurement. It should be pointed out here that this method has been used to confirm the occupation status of Ca cation in $BaFeO_{3-\delta}$ [22]. Fig. 2 presents the core level XPS spectra of Ba 3d, Mg 1s, O 1s and Ca 2p of BFM-Ca membrane at room temperature. Fig.2b shows that the Ba 3d consists of two peaks at 778.32 and 793.62 eV which were assigned to Ba atoms in the BFM-Ca perovskite structure [30], while two subpeaks at about 779.56 and 794.86 eV probably related to relaxed Ba phase caused by oxygen vacancies and other residual defects [31]. It was clear that the Mg had a single chemical environment in the cubic perovskite structure of BFM-Ca. The O 1s spectra in Fig.2d presented three peaks, with binding energy (BE) value at 528.3, 529 and 530.9 eV. The peak at 528.3 eV was attributed to O^{2-} lattice oxygen species, while the peaks at 529 and 530.9 eV correspond to adsorbed oxygen species at the surface (i.e. O_2^{2-}, O^-) and OH^-/CO_3^{2-}, respectively [32]. Remarkably, it can be seen from Fig.2e that each of the Ca 2p1/2 and Ca 2p3/2 peaks are fitted well with two peaks separated by around 0.93 eV, indicating two different chemical environments of Ca i.e., A-site with 12-fold coordination as well as B-site with 6-fold coordination in BFM-Ca material. The Mg KLL Auger peak at 348.3 eV [33] was also included in the image. The Ca 2p doublet at the lower binding energy region with relatively higher intensities were designated as Ca atom substituted at Fe site in BFM-Ca [34]. The higher binding

energy peaks, i.e. 349.2 and 345.7 eV, could be assigned to Ca atom at the A-site of BFM-Ca perovskite [35, 36]. Such A-site substitution of Ca dopant in BFM-Ca oxide will cause B-site cation deficiency which may result in the formation of impurity phases and have some effect on the oxygen permeability of BFM-Ca membrane,[37] which will be discussed separately below.

These results indicate that the codoped $BaFe_{0.9}Mg_{0.05}X_{0.05}O_{3-\delta}$ (X= Ce, Ca) oxide can still adopt cubic perovskite structure when the doping ion has a larger size than Zr^{4+}. But, it was found that the largest Ca dopant may not only occupy the B-site of the perovskite structure but also tend to incorporate onto the A-site. Therefore, the occupation status of X cation in BFM was related to the radius of doping ion, which is in accordance with the previous studies [27-29].

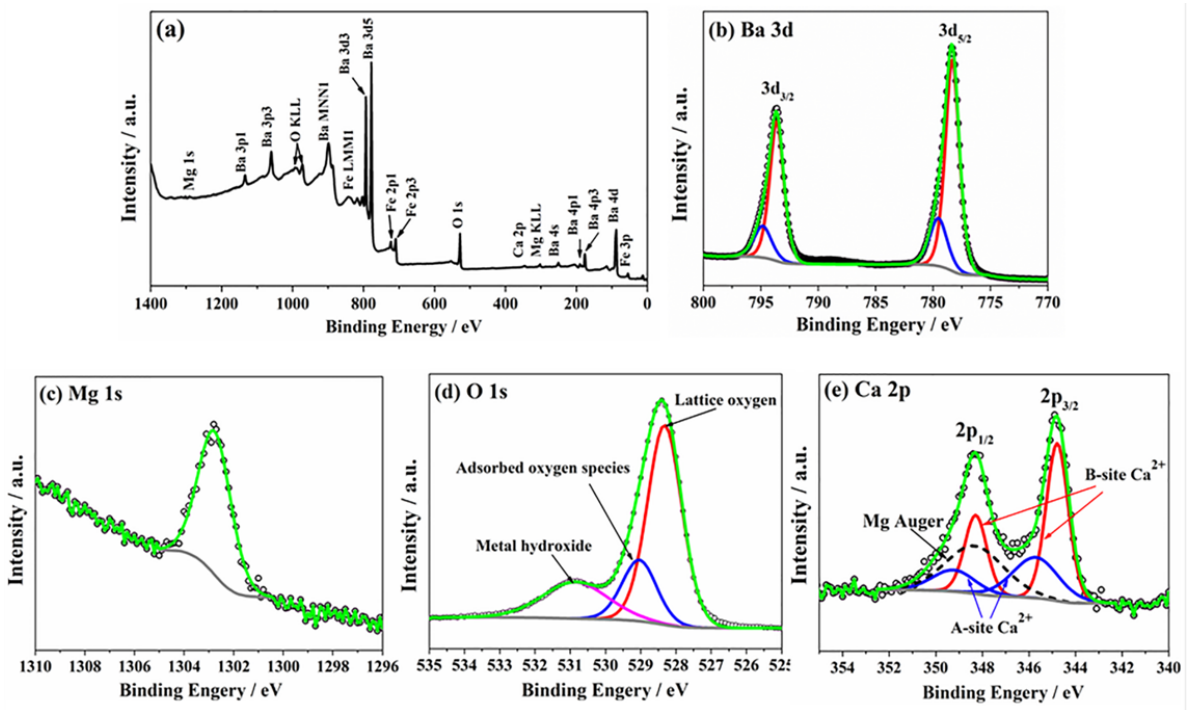

Fig. 2. XPS results of $BaFe_{0.9}Mg_{0.05}Ca_{0.05}O_{3-\delta}$ (BFM-Ca) membrane (a), Ba 3d (b), Mg 1s (c), O 1s (d) and Ca 2p (e).

3.2 Phase stability

Good phase stability in a wide oxygen partial pressure range is an essential requirement for air separation process using oxygen transport membrane, since one side of the membrane is always exposed to atmospheres with low oxygen partial pressure. To gain insight into the effect of X doping on the phase stability of BFM membrane, BFM samples doped with Zr, Ce and Ca cations were heat-treated at 900 °C for 24 h under an argon atmosphere (i.e. $pO_2 \approx 10^{-5}$ bar) and then examined by means of XRD and SEM. As shown in Fig. 3, Ar-treated BFM-Ce and BFM-Ca membranes maintained their cubic perovskite structure without new phases, the same as that of BFM-Zr membrane, indicating the good phase stability under Ar atmosphere. Note that no additional phases were observed for the treated BFM-Ca membrane even if there may be some calcium ion at the Ba site of the lattice. Thus, it could be expected that all three BFM-X membranes are capable of long-term operation for air separation. Fig.4 presents the morphology of these membranes before and after annealing under argon atmosphere. All the treated BFM-X membranes still had clear grain boundaries with dense structure. No impurity phase was observed on the surface of the treated membranes. These observations are consistent with the XRD results in Fig.3, revealing good phase stability under low oxygen partial pressure atmospheres.

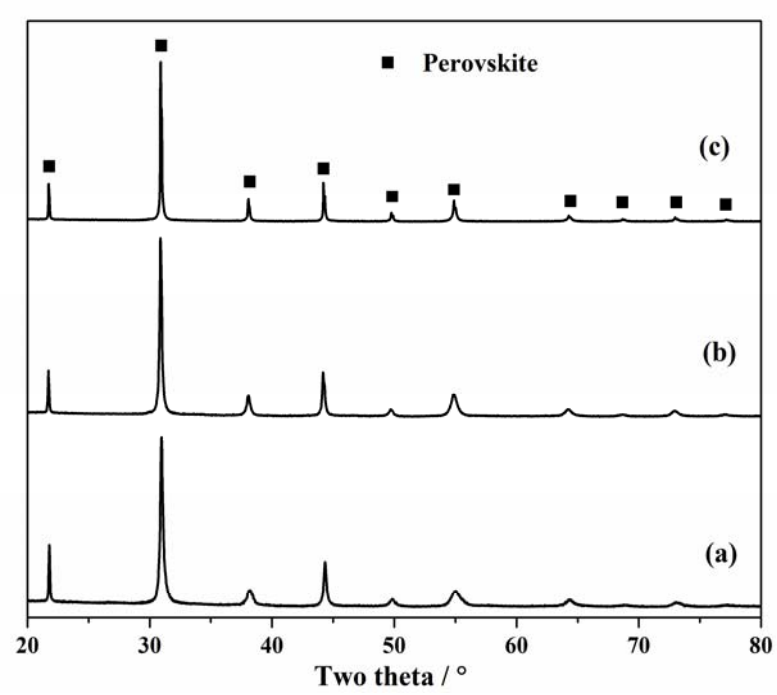

Fig. 3 XRD patterns of (a) BFM-Zr, (b) BFM-Ce and (c) BFM-Ca membranes treated at 900 °C for 24 h under Ar atmosphere.

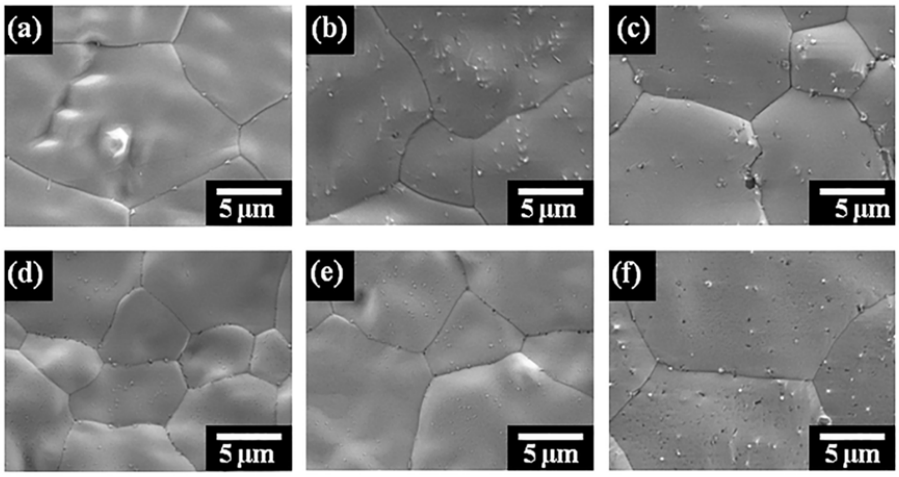

Fig. 4 SEM images of (a, d) BFM-Zr, (b, e) BFM-Ce and (c, f) BFM-Ca membranes before (a-c) and after (d-f) Ar treatment.

For a more precise evaluation of the effect of X doping on the stability of BFM, the weight alteration (gain or loss) behaviors of BFM-X oxides were measured by TG under the temperature-programmed conditions in air and argon atmospheres, the results of which are shown in Fig.5. All BFM-X samples exhibited a similar trend, i.e. 1) a gradual weight loss in air; 2) a fast initial weight loss followed by a continuous and steady decrease in argon; 3) a weight gain with a plateau after exposure to air once again. The initial weight loss should be associated with the removal of adsorbed species such as H_2O and CO_2 from the ambient atmosphere after synthesis below 400 °C, while the continuous weight loss at higher temperatures was attributed to the thermal reduction of Fe ions and the release of lattice oxygen in BFM-X structure [22]. Once the atmosphere was changed to Ar, the oxygen partial pressure of the exposure atmosphere decreased significantly, which caused additional chemical reduction of Fe ions, resulting in a fast loss of lattice oxygen [38]. Thereafter, all BFM-X samples showed a smooth monotonic weight loss in Ar, reflecting another slight and gradual loss of lattice oxygen without new phases formation, as confirmed by XRD results in Fig.3. When the atmosphere was shifted back to air, oxygen uptake caused re-oxidation of iron ions and thus resulted in weight gain of BFM-X samples. After this oxidation stage, the weights of BFM-X gradually got back to the stabilized value during the previous air-exposure period. This provided further evidence that BFM-X membranes were chemically stable under Ar atmosphere. Among these three materials, the weight loss of BFM-Ce in Air and Ar atmosphere was relatively greater. This may be attributed to the extra oxygen loss by thermal and chemical reductions of cerium ions ($Ce^{4+} + e \rightarrow Ce^{3+}$) at high temperatures [23, 24], thus after Ar exposure-period the weight gain to the steady state of BFM-Ce oxide took a longer time than that of BFM-Zr and BFM-Ca. To fulfill the electric neutrality criteria, the Ce^{3+} ions from the reduction should facilitate the formation of oxygen

vacancies and enhance the oxygen ion conductivity in BFM-Ce. Overall, after a redox cycle between air and argon at 900 °C, all BFM-X oxides presented almost completely reversible weight changes, indicating that these oxides had good phase stability under low oxygen partial pressure argon atmosphere.

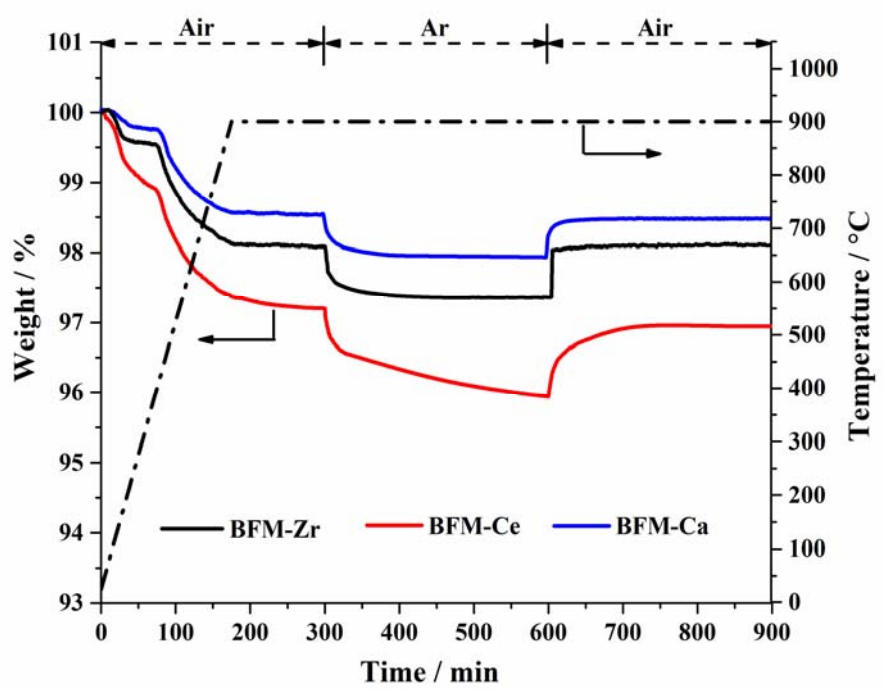

Fig. 5 TG analysis of BFM-X (X = Zr, Ce and Ca) oxides in Air and Ar atmospheres.

Derived from TG data shown in Fig.5, the changes of the oxygen non-stoichiometric (Δδ) of BFM-X oxides with temperature in air were calculated according to eq.2.

$$\Delta\delta = \frac{\Delta w\, M_S}{M_O\, w_S} \qquad \text{(eq.2)}$$

where Δw is the weight change of the specimen, w_S the initial specimen weight, M_O the oxygen atomic weight, and M_S denotes the molecular formula weight of the specimen. As shown in Fig.6, the Δδ values of BFM-X were found to increase gradually with increasing temperature

from 200 to 900 °C in air. Throughout this temperature range, the variation of Δδ for BFM-Ce was the largest, indicating that more oxygen vacancies were produced with increasing temperature. This suggested that the formation energy of oxygen vacancies in BFM-Ce was low, which is expected to contribute to the improved oxygen permeability of BFM-Ce membrane. However, please note that the oxygen ionic conductivity of perovskite-type oxide at specific temperature predominantly depends on the formation energy as well as ion migration energy barrier of the oxygen vacancy [39]. On the other hand, BFM-Ca and BFM-Zr had relatively smaller variations of Δδ, indicating that less amount of lattice oxygen was released at high temperatures and hence they may possess higher phase stability than BFM-Ce [40]. This could be evidenced by the phase changes of BFM-X membranes subjected to a 3 vol.% H_2/Ar treatment at 900 °C for 10 h. As shown in Fig. 7, the cubic perovskite phase of the treated BFM-Ca and BFM-Zr membranes still remained with a small amount of metallic Fe (PDF# 87-0721) and $Ba_3Fe_2O_6$ (PDF# 25-1477) phases, respectively. In contrast, BFM-Ce exhibited a severe degradation of the perovskite phase after H_2/Ar treatment, indicating a lower phase stability. Therefore, it could be concluded that all of these three codoped BFM-X membranes exhibited good phase stability under argon atmosphere, showing promise for oxygen separation from air. However, rather than BFM-Ca and BFM-Zr, a severe phase degradation of BFM-Ce perovskite occurred in a strongly reducing atmosphere (i.e. H_2/Ar), which may be attributed to the chemical reduction of cerium ion.

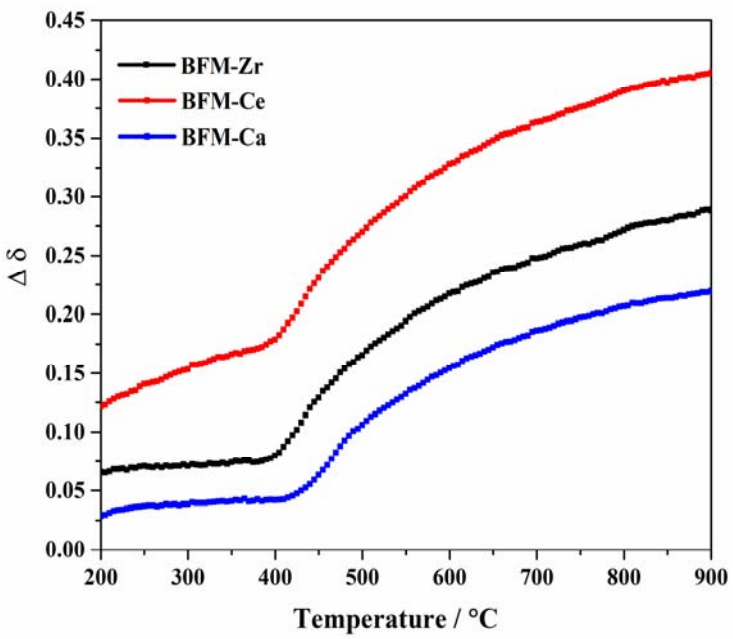

Fig. 6 Oxygen non-stoichiometry change of BFM-X (X = Zr, Ce and Ca) oxides in air with temperature.

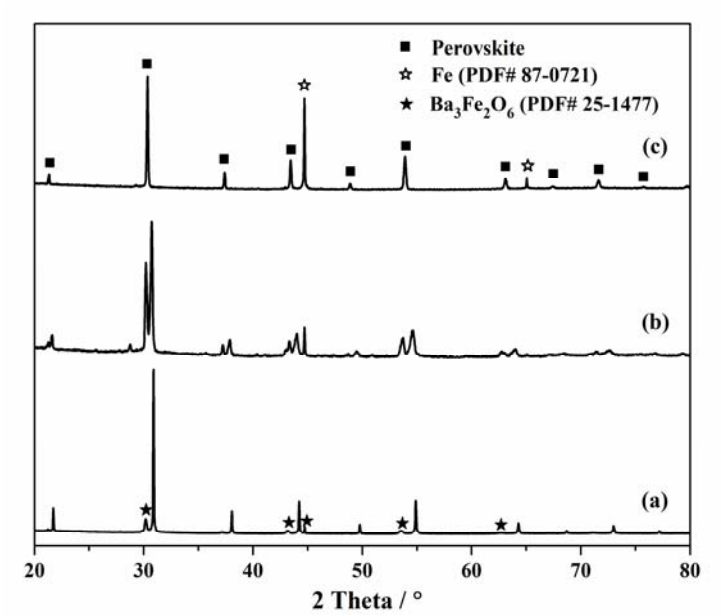

Fig. 7 XRD patterns of (a) BFM-Zr, (b) BFM-Ce and (c) BFM-Ca codoped membranes annealed at 900 °C in 3 vol.% H_2/Ar for 10 h.

3.3 Electrical conductivity and oxygen permeation behaviors

The electrical conductivities of BFM-X were measured in air as functions of temperature. For most of the OTMs, the electrical conductivity is usually at least one or two orders of magnitude larger than the ionic conductivity.[41] Thus, the electrical conductivities of BFM-X samples in air can be assumed to be the electronic conductivity alone. As shown in Fig.8a, the conductivities of BFM-X membrane decrease gradually with increasing the temperature from 450 to 900 °C, which is due to the release of lattice oxygen and thereby partial annihilation of electron defects. Among BFM-X membranes, BFM-Ce has the highest conductivity, probably attributed to the Zerner double exchange via Ce^{4+} and Ce^{3+}.[26] The lowest conductivity of BFM-Ca may result from the impurity phases and B-site cation deficiency because of A-site substitution of Ca dopant deduced from the XPS studies in Fig.2.

The oxygen permeation flux was measured on the BFM-X (X= Zr, Ce, Ca) membranes with 1.0 mm thickness under conditions of 50/250 cm^3 min^{-1} cm^{-2} Ar/Air oxygen partial pressure gradient, as shown in Fig. 8b. The mechanical strength of BFM membranes was very poor, which did not allow us to measure the oxygen permeation performance. For all BFM-X membranes, the oxygen permeation fluxes increase with increasing temperatures, indicating a thermal activated process of the oxygen permeation. Among these membranes, the oxygen permeation flux of BFM-Ce membrane exhibits the highest value in the temperature range from 800 to 1000 °C, which is in accordance with the highest electrical conductivity as shown in Fig. 8a. Comparing BFM-Zr and BFM-Ce membranes, the higher oxygen permeability of BFM-Ce is probably attributed that the lower valence Ce^{3+} ions in BFM-Ce facilitate the formation of oxygen vacancies and enhance oxygen ion conductivity in the membrane. This is supported by the previous study about the effect of Ce doping on oxygen permeability of $BaFe_{1-x}Ce_xO_{3-\delta}$ [18].

In the case of BFM membrane doped by Ca^{2+} (ionic radius = 1.0 Å), BFM-Ca membrane exhibits the lowest oxygen permeation flux, which may be related to A-site substitution of Ca cation in BFM-Ca structure as inferred in Fig.2, resulting in the formation of B-site cation deficiency and impurity phases for low mixed conductivity. Accordingly, the activation energies for oxygen permeation of BFM-X membranes decrease in the order of Ca > Zr > Ce, having an opposite behavior of oxygen permeation rate (Fig. 8c). Especially for BFM-Ce, it has a lower activation energy for oxygen permeation than 5% Ce-doped $BaFe_{0.95}Ce_{0.05}O_{3-\delta}$ [18], which is expected to result in a higher oxygen permeability under the same experimental conditions. It is concluded that BFM-Ce membrane exhibits the highest oxygen permeability among BFM-X membrane, probably due to the increase in oxygen vacancies because of multiple oxidation state of Ce ions.

The long-term stability of BFM-Ce membrane was then investigated at 900 °C under an Air/Ar gradient. The oxygen permeation flux can remain at about 0.9 cm^3 min^{-1} cm^{-2} for about 150 h with no obvious degradation, as shown in Fig. 8d, indicating the good long-term structural stability of BFM-Ce material. In contrast to easy decomposition of cobalt-based perovskite membranes,[1] the BFM-Ce membrane displays a high stability with good long term operational reliability. These results support that BFM-Ce is a promising oxygen permeation membrane material for air separation.

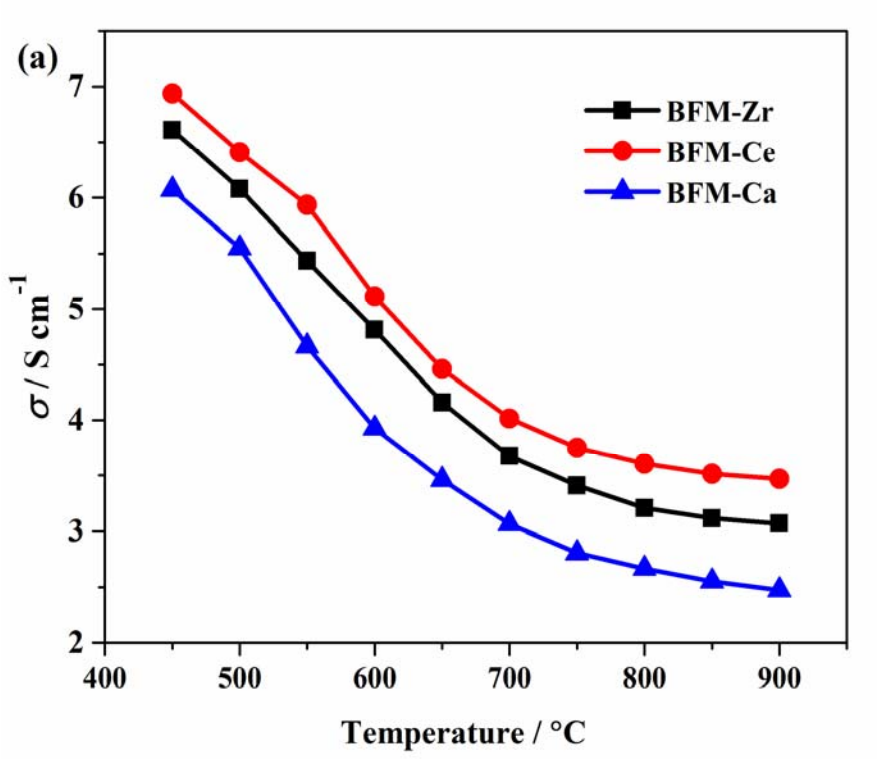
(a)
BFM-Zr
BFM-Ce
BFM-Ca
σ / S cm-1
Temperature / °C

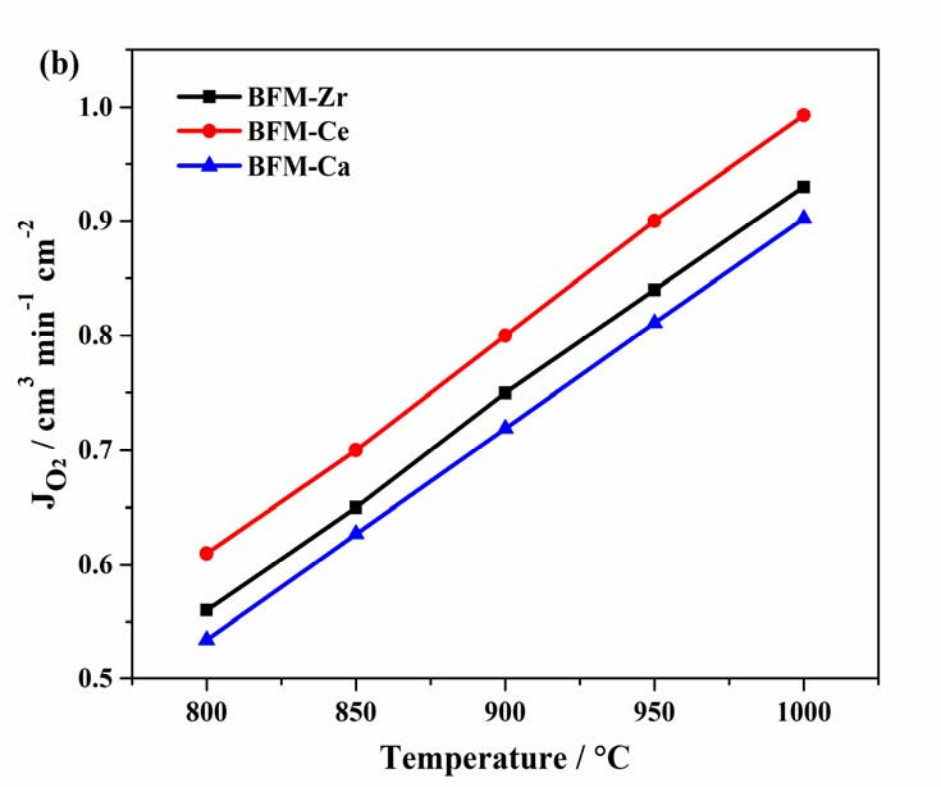
(b)
BFM-Zr
BFM-Ce
BFM-Ca
JO2 / cm3 min-1 cm-2
Temperature / °C

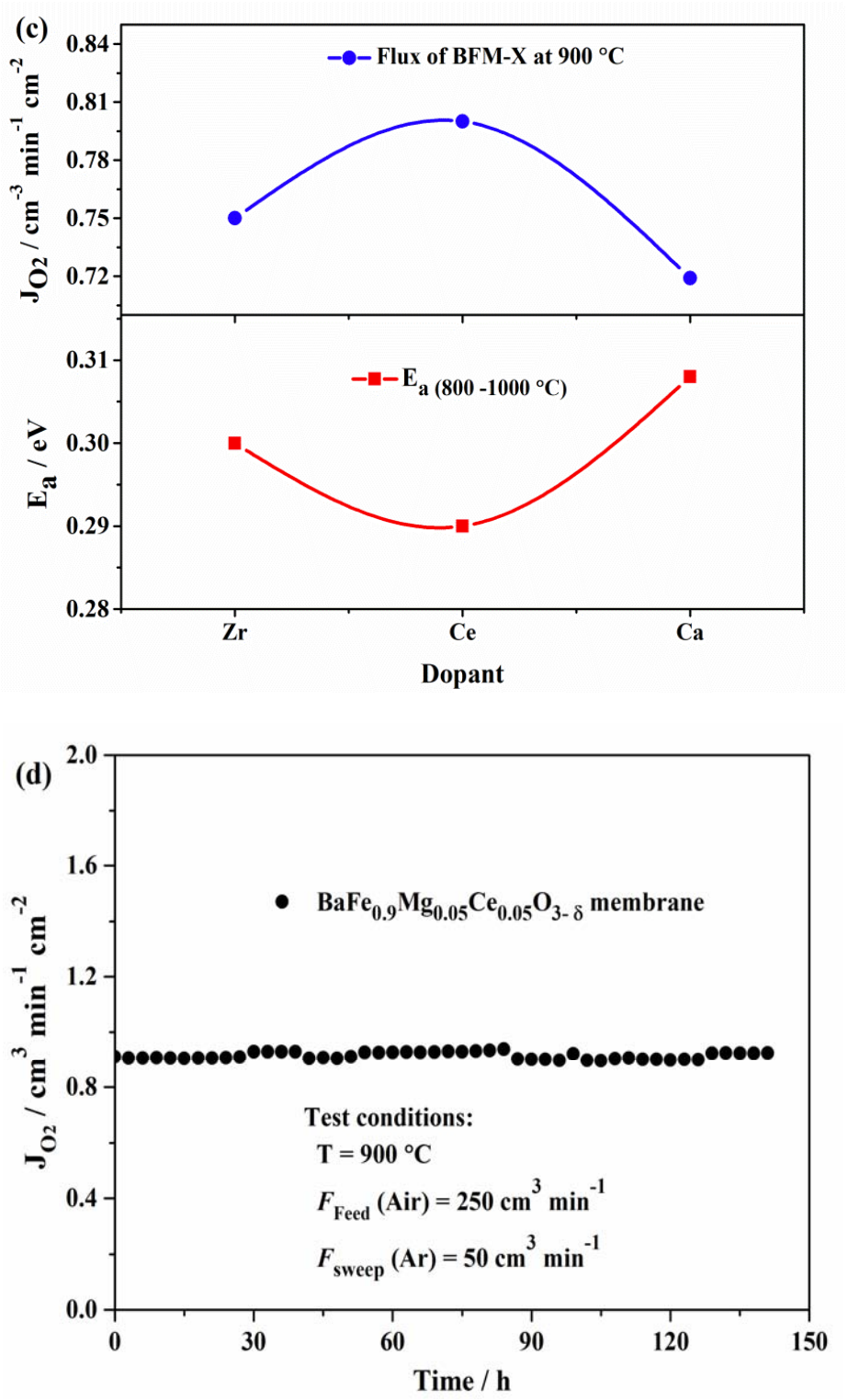

Fig. 8 a) Temperature dependence of electrical conductivity of BFM-X (X = Zr, Ce and Ca) samples in air. b) Temperature dependent oxygen permeation fluxes of BFM-X membranes (X =

Zr, Ce and Ca) with 1.0 mm thickness (F_{air} = 250 cm^3 min^{-1}, F_{Ar} = 50 cm^3 min^{-1}). c) Variation of the calculated activation energies and oxygen permeation fluxes at 900 °C upon doping cation; d) Long term oxygen permeation flux of the $BaFe_{0.9}Mg_{0.05}Ce_{0.05}O_{3-\delta}$ (BFM-Ce) membrane with 0.71 mm thickness at 900 °C.

4. Conclusions

B-site codoped $BaFe_{0.9}Mg_{0.05}X_{0.05}O_{3-\delta}$ (BFM-X = Zr, Ce, Ca) perovskite oxides were synthesized by the EDTA-citric acid combustion method. XRD results revealed that all dopants can be incorporated at the B-site of $BaFe_{0.95}Mg_{0.05}O_{3-\delta}$ with reducing the mismatch between Ba and Fe cations, as a result, the phase transformation from cubic to hexagonal perovskite structure at room temperature was effectively prevented. In particular, Ca 2*p* XPS spectra of BFM-Ca suggested that the relatively larger calcium ion may occupy both the A- and B-site of $BaFe_{0.95}Mg_{0.05}O_{3-\delta}$ lattice. All the codoped BFM-X oxides exhibited good phase stability under argon atmosphere without any phase changes, as verified by XRD, SEM and TG studies. TG analysis also revealed the reduction of cerium ions from 4+ to 3+ in BFM-Ce, being associated with its larger electrical conductivity and higher oxygen permeability. The lowest oxygen permeation fluxes of BFM-Ca membrane is due to the ionic radii mismatch between Ca^{2+} and Fe^{4+}, leading to A-site substitution of Ca cations and B-site cation deficiency in BFM-Ca oxide. Overall, among these codoped membranes, BFM-Ce gave the highest oxygen permeability and good long term operation stability at high temperatures, thus it is recommended as a promising membrane material for air separation.

Published in Separation and Purification Technologies 220 (2019) 176-182

Acknowledgments

This work was supported by National Natural Science Foundation of China and 2016 Jülich-OCPC-Program (Grant No. 21506237, 91645124), the International Partnership Program of Chinese Academy of Sciences (Grant No. 153937KYSB20180048) and Shandong Provincial Key R&D Project (2018GSF117031). The authors also acknowledge Dr. Frank Tietz and Stefan Heinz for their supports on TGA and oxygen permeation measurements.

References

[1] F. Liang, H. Jiang, H. Luo, J. Caro, A. Feldhoff, Phase stability and permeation behavior of a dead-end $Ba_{0.5}Sr_{0.5}Co_{0.8}Fe_{0.2}O_{3-\delta}$ tube membrane in high-purity oxygen production, Chem. Mater. 23 (2011) 4765-4772.

[2] X. Zhang, J. Motuzas, S. Liu, J.C. Diniz da Costa, Zinc-doped BSCF perovskite membranes for oxygen separation, Sep. Purif. Tech. 189 (2017) 399-404.

[3] H. Luo, K. Efimov, H. Jiang, A. Feldhoff, H. Wang, J. Caro, CO_2-stable and cobalt-free dual-phase membrane for oxygen separation, Angew. Chem. Int. Ed. 50 (2011) 759-63.

[4] W. Liang, Z. Cao, G. He, J. Caro, H. Jiang, Oxygen transport membrane for thermochemical conversion of water and carbon dioxide into synthesis gas, ACS Sustain. Chem. Eng. 5 (2017) 8657-8662.

[5] M. Tou, R. Michalsky, A. Steinfeld, Solar-driven thermochemical splitting of CO_2 and in situ separation of CO and O_2 across a ceria redox membrane reactor, Joule 1 (2017) 146-154.

[6] H. Jiang, Z. Cao, S. Schirrmeister, T. Schiestel, J. Caro, A coupling strategy to produce hydrogen and ethylene in a membrane reactor, Angew. Chem. Int. Ed. 49 (2010) 5656-5660.

[7] G. He, T. Hu, H. Zhou, F. Liang, S. Baumann, W.A. Meulenberg, H. Jiang, Syngas production by biogas reforming in a redox-stable and CO_2-tolerant oxygen transporting membrane reactor, Ind. Eng. Chem. Res. 56 (2017) 10134-10141.

[8] L. Qiu, T.H. Lee, L.M. Liu, Y.L. Yang, A.J. Jacobson, Oxygen permeation studies of $SrCo_{0.8}Fe_{0.2}O_{3-\delta}$, Solid State Ionics 76 (1995) 321-329.

[9] Z. Shao, W. Yang, Y. Cong, H. Dong, J. Tong, G. Xiong, Investigation of the permeation behavior and stability of a $Ba_{0.5}Sr_{0.5}Co_{0.8}Fe_{0.2}O_{3-\delta}$ oxygen membrane, J. Membr. Sci. 172 (2000) 177-188.

[10] Y. Tsuruta, T. Todaka, H. Nisiguchi, T. Ishihara, Y. Takita Mixed electronic-oxide ionic conductor of Fe-doped La(Sr)GaO_3 perovskite oxide for oxygen permeating membrane, Electrochem. Solid State Lett. 4 (2001) E13-E15.

[11] Y. Wei, Q. Liao, Z. Li, H. Wang, Enhancement of oxygen permeation through U-shaped K_2NiF_4-type oxide hollow fiber membranes by surface modifications, Sep. Purif. Tech. 110 (2013) 74-80.

[12] K. Efimov, T. Halfer, A. Kuhn, P. Heitjans, J. Caro, A. Feldhoff, Novel cobalt-free oxygen-permeable perovskite-type membrane, Chem. Mater. 22 (2010) 1540-1544.

[13] Y. Teraoka, H. Shimokawa, C.Y. Kang, H. Kusaba, K. Sasaki, Fe-based perovskite-type oxides as excellent oxygen-permeable and reduction-tolerant materials, Solid State Ionics 177 (2006) 2245-2248.

[14] F. Schulze-Küppers, S.F.P. ten Donkelaar, S. Baumann, P. Prigorodov, Y.J. Sohn, H.J.M. Bouwmeester, W.A. Meulenberg, O. Guillon, Structural and functional properties of $SrTi_{1-x}Fe_xO_{3-\delta}$ ($0 \leqslant x \leqslant 1$) for the use as oxygen transport membrane, Sep Purif Tech 147 (2015) 414-421.

[15] G. He, Z. Cao, W. Liang, Y. Zhang, X. Liu, J. Caro, H. Jiang, Codoping strategy to improve stability and permeability of $Ba_{0.6}Sr_{0.4}FeO_{3-\delta}$-based perovskite membranes, Ind. Eng. Chem. Res. 55 (2016) 10386-10393.

[16] X. Liu, H. Zhao, J. Yang, Y. Li, T. Chen, X. Lu, W. Ding, F. Li, Lattice characteristics, structure stability and oxygen permeability of $BaFe_{1-x}Y_xO_{3-\delta}$ ceramic membranes, J. Membr. Sci. 383 (2011) 235-240.

[17] K. Watanabe, D. Takauchi, M. Yuasa, T. Kida, K. Shimanoe, Y. Teraoka, N. Yamazoe, Oxygen permeation properties of Co-free perovskite-type oxide membranes based on $BaFe_{1-y}Zr_yO_{3-\delta}$, J. Electrochem. Soc. 156 (2009) E81-E85.

[18] X. Zhu, H. Wang, W. Yang, Structural stability and oxygen permeability of cerium lightly doped $BaFeO_{3-\delta}$ ceramic membranes, Solid State Ionics 177 (2006) 2917-2921.

[19] H. Wang, C. Tablet, A. Feldhoff, J. Caro, A cobalt-free oxygen-permeable membrane based on the perovskite-type oxide $Ba_{0.5}Sr_{0.5}Zn_{0.2}Fe_{0.8}O_{3-\delta}$, Adv. Mater. 17 (2005) 1785-1788.

[20] J. Martynczuk, F. Liang, M. Arnold, V. Šepelák, A. Feldhoff, Aluminum-doped perovskites as high-performance oxygen permeation materials, Chem. Mater. 21 (2009) 1586-1594.

[21] S.R. D., Revised effective ionic radii and systematic studies of interatomic distances in halides and chalcogenides, Acta Cryst. A 32 (1976) 751-767.

[22] Y. Lu, H. Zhao, K. Li, X. Du, Y. Ma, X. Chang, N. Chen, K. Zheng, K. Swierczek, Effective calcium doping at the B-site of $BaFeO_{3-\delta}$ perovskite: towards low-cost and high-performance oxygen permeation membranes, J. Mater. Chem. A 5 (2017) 7999-8009.

[23] V. Ramasamy,G. Vijayalakshmi, Effect of Zn doping on structural, optical and thermal properties of CeO_2 nanoparticles, Superlattices Microst. 85 (2015) 510-521.

[24] G. Montes-Hernandez, R. Chiriac, N. Findling, F. Toche, F. Renard, Synthesis of ceria (CeO_2 and CeO_{2-x}) nanoparticles via decarbonation and Ce(III) oxydation of synthetic bastnäsite ($CeCO_3F$), Mater. Chem. Phys 172 (2016) 202-210.

[25] S. Baumann, F. Schulze-Küppers, S. Roitsch, M. Betz, M. Zwick, E.M. Pfaff, W.A. Meulenberg, J. Mayer, D. Stöver, Influence of sintering conditions on microstructure and oxygen permeation of $Ba_{0.5}Sr_{0.5}Co_{0.8}Fe_{0.2}O_{3-\delta}$ (BSCF) oxygen transport membranes, J. Membr. Sci. 359 (2010) 102-109.

[26] P. Zeng, Z. Shao, S. Liu, Z.P. Xu, Influence of M cations on structural, thermal and electrical properties of new oxygen selective membranes based on $SrCo_{0.95}M_{0.05}O_{3-\delta}$ perovskite, Sep. Purif. Tech. 67 (2009) 304-311.

[27] H. Donglin, S. Kozo, U. Tetsuya, Dopant site occupancy and chemical expansion in rare earth□doped barium zirconate, J. Am. Ceram. Soc. 97 (2014) 643-650.

[28] M.T. Buscaglia, V. Buscaglia, M. Viviani, P. Nanni, M. Hanuskova, Influence of foreign ions on the crystal structure of $BaTiO_3$, J. Eur. Ceram. Soc. 20 (2000) 1997-2007.

[29] L.A. Xue, Y. Chen, R.J. Brook, The influence of ionic radii on the incorporation of trivalent dopants into $BaTiO_3$, Mater. Sci. Eng. B 1 (1988) 193-201.

[30] V. Craciun,R.K. Singh, Characteristics of the surface layer of barium strontium titanate thin films deposited by laser ablation, Appl. Phys. Lett. 76 (2000) 1932-1934.

[31] Z. Quan, B. Zhang, T. Zhang, T. Guo, R. Pan, J. Jiang, Etching characteristics and plasma-induced damage of $Ba_{0.6}5Sr_{0.35}TiO_3$ thin films etched in $CF_4/Ar/O_2$ plasma, Microelectron. Eng. 84 (2007) 631-637.

[32] J.-I. Jung,D.D. Edwards, X-ray photoelectron (XPS) and diffuse reflectance infra fourier transformation (DRIFT) study of $Ba_{0.5}Sr_{0.5}Co_xFe_{1-x}O_{3-\delta}$ (BSCF: x=0–0.8) ceramics, J. Solid State Chem. 184 (2011) 2238-2243.

[33] V.P. Zakaznova-Herzog, H.W. Nesbitt, G.M. Bancroft, J.S. Tse, High resolution core and valence band XPS spectra of non-conductor pyroxenes, Surf. Sci. 600 (2006) 3175-3186.

[34] A. Dutta, S. Saha, P. Kumari, T.P. Sinha, S. Shannigrahi, Crystal structure and X-ray photoemission spectroscopic study of A_2LaMO_6 [A=Ba, Ca; M=Nb, Ta], J. Solid State Chem. 229 (2015) 296-302.

[35] X. Liu, W. Su, Z. Lu, Study on valence state and electrical conductivity of $La_{1-x}Ca_xCrO_3$, J. Phys. Chem. Solids 62 (2001) 1919-1921.

[36] N.H. Batis, P. Delichere, H. Batis, Physicochemical and catalytic properties in methane combustion of $La_{1-x}Ca_xMnO_{3\pm y}$ ($0\leq x\leq 1$; $-0.04\leq y\leq 0.24$) perovskite-type oxide, Appl. Catal. A: Gen. 282 (2005) 173-180.

[37] L. Ge, R. Ran, K. Zhang, S. Liu, Z. Shao, Oxygen selective membranes based on B-site cation-deficient $(Ba_{0.5}Sr_{0.5})(Co_{0.8}Fe_{0.2})_yO_{3-\delta}$ perovskite with improved operational stability, J. Membr. Sci. 318 (2008) 182-190.

[38] T. Gotsch, L. Schlicker, M.F. Bekheet, A. Doran, M. Grunbacher, C. Praty, M. Tada, H. Matsui, N. Ishiguro, A. Gurlo, B. Klotzer, S. Penner, Structural investigations of $La_{0.6}Sr_{0.4}FeO_{3-\delta}$ under reducing conditions: kinetic and thermodynamic limitations for phase transformations and iron exsolution phenomena, RSC Adv. 8 (2018) 3120-3131.

[39] T. Ishigaki, S. Yamauchi, K. Kishio, J. Mizusaki, K. Fueki, Diffusion of oxide ion vacancies in perovskite-type oxides, J. Solid State Chem. 73 (1988) 179-187.

[40] M. Al Daroukh, V.V. Vashook, H. Ullmann, F. Tietz, I. Arual Raj, Oxides of the AMO_3 and A_2MO_4-type: structural stability, electrical conductivity and thermal expansion, Solid State Ionics 158 (2003) 141-150.

[41] D. Xu, F. Dong, Y. Chen, B. Zhao, S. Liu, M.O. Tade, Z. Shao, Cobalt-free niobium-doped barium ferrite as potential materials of dense ceramic membranes for oxygen separation, J. Membr. Sci. 455 (2014) 75-82.

Published in Separation and Purification Technologies 220 (2019) 176-182

Highlights

- Cobalt-free, Fe-based $BaFe_{0.9}Mg_{0.05}X_{0.05}O_{3-\delta}$ (X=Zr, Ce, Ca) perovskite oxides.
- Only 5 mol.% of X ion substitution causes the phase change of $BaFe_{0.95}Mg_{0.05}O_{3-\delta}$.
- BFM-Ce gives the highest oxygen permeability in the investigated temperature range.
- BFM-Ce exhibits good long-term operation stability under air/argon gradient.